Chaos, Solitons and Fractals 153 (2021) 111537

Contents lists available at ScienceDirect

Chaos, Solitons and Fractals

Nonlinear Science, and Nonequilibrium and Complex Phenomena

journal homepage: www.elsevier.com/locate/chaos

Frontiers

Global and localised temporal structures in driven ring quantum cascade lasers

F. Prati[a,*], L.A. Lugiato[a], A. Gatti[a,b], L. Columbo[c], C. Silvestri[c], M. Gioannini[c], M. Brambilla[d], M. Piccardo[e], F. Capasso[f]

[a] Dipartimento di Scienza e Alta Tecnologia, Universitá dell'Insubria, Via Valleggio 11, Como 22100, Italy
[b] Istituto di Fotonica e Nanotecnologie del CNR-IFN, Piazza Leonardo da Vinci 32, Milano 20133, Italy
[c] Dipartimento di Elettronica e Telecomunicazioni, Politecnico di Torino, Corso Duca degli Abruzzi 24, Torino 10129, Italy
[d] Dipartimento di Fisica Interateneo and CNR-IFN, Universitá e Politecnico di Bari, Via Amendola 173, Bari 70123, Italy
[e] Center for Nano Science and Technology, Fondazione Istituto Italiano di Tecnologia, Via Giovanni Pascoli 70, Milano 20133, Italy
[f] Harvard John A. Paulson School of Engineering and Applied Sciences, Harvard University, Cambridge, MA, USA

ARTICLE INFO

Article history:
Received 30 July 2021
Accepted 17 October 2021

Keywords:
Pattern formation
Cavity solitons
Snaking
Quantum cascade lasers

ABSTRACT

Starting from a full set of effective Maxwell-Bloch equations for a ring quantum cascade laser in the limit of fast material dynamics we derive a new set of equations which require a considerably lower numerical load because they evolve on the time scale of the electric field. With the further assumption of laser very close to threshold the equations take the form of the generalised Lugiato-Lefever equation. Using the latter, we study the formation and stability of multi-peaked localised structures which can be regarded as portions of a global pattern and exhibit a snaking structure.

1. Introduction

Since the mid seventies of the previous century the analysis of unstable phenomena in nonlinear optical systems has been the object of intensive studies, both theoretical and experimental. These investigations have encompassed both instabilities that lead to spontaneous temporal oscillations in the longitudinal direction of light propagation (see e.g. [1–4]) and instabilities that produce the spontaneous onset of a spatial structure in the planes orthgonal to the propagation direction (see e.g [5–7]). An immense variety of ordered or chaotic patterns in time, in space or in space-time have been discovered. Tito Arecchi, a much estimated colleague and dear friend, has been one of the authors who mostly contributed to these developments, at a worldwide level, and it is now a great pleasure of ours to dedicate him this paper of ours.

The study of instabilities, and of the temporal/spatial patterns they produce, is ubiquitous in the vast area on nonlinear dynamics that includes, for example, hydrodynamics, nonlinear chemical reactions or biology. These phenomena represent the general object of study of Haken's synergetics [8] and of Prigogine's theory of dissipative structures [9]. The case of optics is especially interesting for a number of reasons: first, it studies systems whose dynamics is governed by the fundamental laws of radiation-matter interaction, second, optical sytems are very fast and have a large frequency bandwidth, hence they lend themselves naturally for applications, for instance to telecommunications and to information technology.

The usefulness of the investigations on instabilities and pattern formation in nonlinear optical systems is demonstrated especially by the realization of microresonator-based Kerr frequency combs (KFCs), such as those generated by cavity solitons [10,11]. Their behaviour is governed by an equation [called Lugiato-Lefever equation (LLE) in the following] formulated in 1987 [12], 20 years before the discovery of Kerr frequency combs: for a discussion of the LLE and its connections with microresonator frequency combs see [13–17]. Combined with the ability to miniaturize and integrate on chip, Kerr frequency combs have been already found applications, e.g., in dual-comb spectroscopy, frequency synthesis, low-noise microwave generation, laser frequency ranging and astrophysical spectrometer calibration [15,17,18].

Recently frequency combs have been observed in ring Quantum Cascade Lasers (QCLs) [19,20], unipolar semiconductor lasers first realized in 1994 [21] emitting in the midinfrared and terahertz regions. QCLs have raised a noteworthy interest, especially in midinfrared spectroscopy and sensing [22,23] because of their tunability and unique physical properties [24,25]. The study of ring QCLs exhibited a number of similarities with KFCs, in particular the mul-

* Corresponding author.
E-mail address: franco.prati@uninsubria.it (F. Prati).

https://doi.org/10.1016/j.chaos.2021.111537
0960-0779/

timode laser instability is produced by the interplay of nonlinear and dispersive effects, as in the modulational instability in passive microresonators.

In [19] it is shown that, assuming fast material dynamics compared with that of the optical field envelope (hypothesis very well justified for QCLs [25]) and near-threshold operation, the behaviour of the QCL is described by a complex Ginzburg-Landau equation, where the two coefficients of the equation are controlled by the linewidth enhancement factor [26] (LEF) or alpha-factor and by the group velocity dispersion. A CGLE was also formulated in [27] in 1988, and can be regarded as the active counterpart of the LLE, that was formulated for passive driven resonators.

In a recent paper [28] we unified the description of frequency combs in passive and active systems by introducing a Generalized LLE (GLLE in the following), corresponding to the simplest equation that includes the passive and the active LLE as special cases. Since in the passive case the resonator is driven by an external coherent field, the GLLE leads naturally to consider the configuration of a ring QCL with injected signal. This has been studied in [28] and also in [29] where the existence of highly correlated spatial patterns (also referred to as 'global patterns') in form of Turing Rolls and Localised Structures (LSs) in the form of Temporal Solitons (or Cavity Solitons (CSs)) was predicted. While the former are associated with optical frequency combs with repetition rate multiple of the fundamental one given by the cavity FSR and equal to the inverse of the rolls pitch, a CS is characterised by a set of modes with $sech^2$ envelope spaced by the FSR. Finally, by external addressing we numerically demonstrated in [28,29] the possibility to switch on one or more CSs in the intracavity field profile thus modifying up to some extent the associated optical frequency combs features (e.g. repetition rate).

In this paper we propose an alternative derivation of the GLLE (Section 2) and we use it to complete the study of LSs in a coherently driven ring QCL by focusing on the universal phenomenon of LSs snaking.

2. The generalized LLE for a coherently driven QCL, an alternative derivation

Recently, a set of effective semiconductor Maxwell-Bloch equations (ESMBEs) originally introduced in [30] was successfully applied [31] to describe the coherent multimode dynamics of QCL. The set of ESMBEs in presence of an injected signal E_I, whose frequency ω_0 is taken as reference and is additionally assumed coincident with the laser gain peak, is

$$\tilde{c}\frac{\partial E}{\partial z}+\frac{\partial E}{\partial t}=\frac{1}{\tau_p}\left[-(1+i\theta_c)E+E_I+P+i\beta|E|^2E-i\tilde{c}^3\tau_p\frac{k''}{2}\frac{\partial^2 E}{\partial t^2}\right], \tag{1}$$

$$\frac{\partial P}{\partial t}=\frac{1}{\tau_d}(1-i\alpha)[(1-i\alpha)ED-P], \tag{2}$$

$$\frac{\partial D}{\partial t}=\frac{1}{\tau_e}\left[\mu-D-\frac{1}{2}(E^*P+EP^*)\right], \tag{3}$$

where τ_p, τ_d and τ_e are the damping time of the cavity field, the dephasing time and the carriers lifetime respectively, and μ is the pump parameter scaled to its threshold value. The damping time of the cavity field τ_p is defined as $\tau_p=2L/(\tilde{c}T_{\text{eff}})$ where the effective loss parameter $T_{\text{eff}}=T+\alpha_L L$ accounts for both reflectors losses (T), and distributed waveguide losses ($\alpha_L L$). The variables E, P and D are scaled as in [31] while E_I is introduced as in [16].

In Eq. (1) $\tilde{c}=c/n$ is the group velocity in the active medium, while $\theta_c=(\omega_c-\omega_0)\tau_p$ where ω_c is the cavity resonance closest to ω_0. The α factor in Eq. (2) is the LEF calculated at the gain peak. Finally, β and k'' are the background medium Kerr nonlinearity parameter (relevant, in general, for high pump rates) and the second-order dispersion coefficient due to the waveguide, respectively [32]. Eqs. (1)-(3) satisfy the periodic boundary condition

$$E(0,t)=E(L,t)\,. \tag{4}$$

In the Supplementary Material of [28] it was shown that the ESMBEs can be reduced to a single equation for the electric field in the double limit of fast atomic variables ($\tau_p\gg\tau_d,\tau_e$), which applies well to QCLs, and of laser very close to threshold ($\mu=1+r$ with $r>0$ and $r\ll 1$). The derivation was based on a perturbative expansion of the temporal derivative in the equations for the atomic variables. The final equation, which has the form of a forced complex Ginzburg-Landau equation was named Generalized LLE (GLLE in the following).

In this paper we propose an alternative derivation of the same equation which allows to write an intermediate set of equations where the fast dynamics of the material variables are adiabatically eliminated in the limit $\tau_p\gg\tau_d,\tau_e$. Those equations are valid even for a laser pumped well above threshold, thus in principle allowing for the interpretation of a wider variety of experimental results. When the limit $\mu=1+r$ with $r\ll 1$ is reintroduced, one coherently obtains the GLLE again.

We start by applying to Eqs. (1)-(3) the modal expansion

$$\begin{Bmatrix}E(z,t)\\P(z,t)\\D(z,t)\end{Bmatrix}=\sum_n\begin{Bmatrix}e_n(t)\\p_n(t)\\d_n(t)\end{Bmatrix}e^{ik_n(z-\tilde{c}t)}, \tag{5}$$

with $k_n=(2\pi/L)n$, $n=0,\pm1,\pm2$, allowed by the boundary condition (4). The equations for the slowly varying modal amplitudes e_n, p_n, and d_n read

$$\frac{de_n}{dt}=\frac{1}{\tau_p}\Bigg[-(1+i\theta_c)e_n+E_I\delta_{n,0}+p_n+i\beta\sum_{j,k}e_j^*e_ke_{n+j-k}+i\tilde{c}^3\tau_p\frac{k''}{2}k_n^2e_n\Bigg], \tag{6}$$

$$\frac{dp_n}{dt}-i\tilde{c}k_np_n=\frac{1}{\tau_d}(1-i\alpha)\left[(1-i\alpha)\sum_j e_{n-j}d_j-p_n\right], \tag{7}$$

$$\frac{dd_n}{dt}-i\tilde{c}k_nd_n=\frac{1}{\tau_e}\left[\mu\delta_{n,0}-d_n-\frac{1}{2}\sum_j\left(e_{j-n}^*p_j+e_{n+j}p_j^*\right)\right]. \tag{8}$$

In the limit $\tau_p\gg\tau_d,\tau_e$ of fast atomic variables we can set $dp_n/dt=dd_n/dt=0$ and then we can proceed in two ways. One way consists in solving the linear algebraic system for the p_n, p_n^* and d_n variables to obtain values for p_n at quasi-steady-state to be inserted in Eq. (6) which now describes in a closed form the temporal evolution of each amplitude e_n and thus the laser dynamics.

Alternatively, we can sum again the modes defining the new variables

$$\begin{Bmatrix}\underline{E}(z,t)\\\underline{P}(z)\\\underline{D}(z)\end{Bmatrix}=\sum_n\begin{Bmatrix}e_n(t)\\p_n\\d_n\end{Bmatrix}e^{ik_nz}, \tag{9}$$

where z is the spatial coordinate in a reference frame moving at the light velocity in the cavity, which obey the equations

$$\frac{\partial\underline{E}}{\partial t}=\frac{1}{\tau_p}\left[-(1+i\theta_c)\underline{E}+E_I+\underline{P}+i\beta|\underline{E}|^2\underline{E}-i\tilde{c}^3\tau_p\frac{k''}{2}\frac{\partial^2\underline{E}}{\partial z^2}\right], \tag{10}$$

$$\tilde{c}\frac{d\underline{P}}{dz}=-\frac{1}{\tau_d}(1-i\alpha)[(1-i\alpha)\underline{ED}-\underline{P}], \tag{11}$$

$$\tilde{c}\frac{d\underline{D}}{dz} = -\frac{1}{\tau_e}\left[\mu - D - \frac{1}{2}(\underline{E}^*\underline{P} + \underline{E}\underline{P}^*)\right]. \tag{12}$$

The latter equation set retains the effects of radiation propagation, gain shape and dispersion, associated with multimode dynamics, as opposed to standard adiabatic elimination which implies a flat gain line (since it corresponds to the assumption $\partial D/\partial t = \partial P/\partial t = 0$ in Eqs. (2) and (3)).

Moreover, both sets of Eqs. (6)-(8) with dp_n/dt=dd_n/dt=0 and (10)-(12) can be numerically integrated much more quickly than the original set (1)-(3) because the fast varying variables have been eliminated and much longer time steps can be used. We verified that with $\tau_p = 10^{-10}$ s, $\tau_d = 10^{-13}$ s, and $\tau_e = 2\tau_d$ [consistently with QCL rates (see Tab.1)] the integration time was reduced by a factor of $\simeq$ 100.

A careful check was performed in order to ascertain that Eqs. (10)-(12) could reproduce the results provided by the full model Eqs. (1)-(3). This was done using two different numerical codes (based on modal decomposition and pseudo-spectral method) and we could verify that homogeneous steady states, roll patterns and CSs in the two models were perfectly comparable within a 0.1% accuracy.

As mentioned above, starting from Eqs. (10)-(12) one can easily obtain the generalized LLE of [28,29] in the limit of laser very close to threshold. To this aim we observe that the formal solutions of Eqs. (11) and (12) are

$$\underline{P} = (1 - i\alpha)\left(1 + \frac{\tau_d\tilde{c}}{1 - i\alpha}\frac{\partial}{\partial z}\right)^{-1}\underline{E}\underline{D}, \tag{13}$$

$$\underline{D} = \mu - \frac{1}{2}\left(1 + \tau_e\tilde{c}\frac{\partial}{\partial z}\right)^{-1}(\underline{E}^*\underline{P} + \underline{E}\underline{P}^*). \tag{14}$$

For each mode we have

$$\tau_d\tilde{c}\frac{\partial}{\partial z} \sim \tau_d\tilde{c}k_n = \tau_d\alpha_n, \qquad \tau_e\tilde{c}\frac{\partial}{\partial z} \sim \tau_e\tilde{c}k_n = \tau_e\alpha_n, \tag{15}$$

where $\alpha_n = \tilde{c}k_n$ is the frequency of the n-th sidemode. Assuming $\alpha_n \ll \tau_d^{-1}, \tau_e^{-1}$ we can perform a power expansion of the operators in Eqs. (13) and (14). This holds in the hypothesis, very well verified in most of the experiments, that the number of longitudinal modes involved in the field dynamics span a spectral range much smaller than the FWHM of the gain lineshape.

For the polarization $\underline{P}$ we must include terms up to second order in the expansion in order to keep information about the shape of the susceptibility, and we obtain

$$\underline{P} \simeq (1 - i\alpha)\underline{E}\underline{D} - \tau_d\tilde{c}\frac{\partial(\underline{E}\underline{D})}{\partial z} + \frac{\tau_d^2\tilde{c}^2}{(1 - i\alpha)}\frac{\partial^2(\underline{E}\underline{D})}{\partial z^2} \tag{16}$$

It turns out that the operator in Eq. (14) applies to a quantity of order $|\underline{E}|^2$. If the laser is very close to threshold $|\underline{E}|^2 \ll 1$, we can then keep only the zero order term of the operator and we simply get

$$\underline{D} \simeq \mu(1 - |\underline{E}|^2) \simeq \mu - |\underline{E}|^2, \tag{17}$$

where we have taken into account that $\mu \simeq 1$ (near threshold operation), and insert it in Eq. (16) to finally obtain

$$\underline{P} \simeq (1 - i\alpha)\underline{E}(\mu - |\underline{E}|^2) - \tau_d\tilde{c}\frac{\partial\underline{E}}{\partial z} + \frac{\tau_d^2\tilde{c}^2}{(1 - i\alpha)}\frac{\partial^2\underline{E}}{\partial z^2}. \tag{18}$$

If we insert this expression for $\underline{P}$ in Eq. (10) we obtain

$$\frac{\tau_d}{\tau_p}\tilde{c}\frac{\partial\underline{E}}{\partial z} + \frac{\partial\underline{E}}{\partial t} = \frac{1}{\tau_p}\left[-(1 + i\theta_c)\underline{E} + E_I + \mu(1 - i\alpha)E - (1 - i\alpha)|\underline{E}|^2\underline{E} + \frac{\tau_d^2\tilde{c}^2}{(1 - i\alpha)}\frac{\partial^2\underline{E}}{\partial z^2} + i\beta|\underline{E}|^2\underline{E} - i\tilde{c}^3\tau_p\frac{k''}{2}\frac{\partial^2\underline{E}}{\partial z^2}\right] \tag{19}$$

Again, the derivative with respect to z in the LHS of Eq. (19) is negligible with respect to the term with the derivative with respect to t because for each mode we have

$$\tilde{c}\frac{\partial}{\partial z} \sim \tilde{c}k_n = \alpha_n \sim \frac{\partial}{\partial t} \tag{20}$$

and $\tau_d \ll \tau_p$. If we define $\theta_0 = \theta_c - \mu\beta$, $\Delta = \alpha + \beta$, $d_R = (\tilde{c}\tau_d)^2/(1 + \alpha^2)$ and $d_I = d_R(\alpha + \zeta)$ with $\zeta = -k''\tilde{c}\tau_p\left(1 + \alpha^2\right)/\left(2\tau_d^2\right)$ we can write finally

$$\tau_p\frac{\partial E(z,t)}{\partial t} = E_I - (1 + i\theta_0)E + \mu(1 - i\Delta)\left(1 - |E|^2\right)E + (d_R + id_I)\frac{\partial^2 E}{\partial z^2}, \tag{21}$$

It is convenient to scale the quantities in this way

$$\begin{aligned} \tau &= tr/\tau_p, \\ \eta &= z\sqrt{r/d_R}, \\ F &= E/\sqrt{r}, \\ F_I &= E_I/r^{3/2}, \end{aligned} \tag{22}$$

and define

$$\theta = (\theta_c + \alpha)/r + \alpha, \qquad G = d_I/d_R = \alpha + \zeta, \tag{23}$$

so that Eq. (21) takes the form of the GLLE for the laser [28]

$$\frac{\partial F(\eta,\tau)}{\partial\tau} = F_I + (1 - i\theta)F - (1 - i\Delta)|F|^2F + (1 + iG)\frac{\partial^2 F}{\partial\eta^2}, \tag{24}$$

If we consider the scaling (22), the fact that $r \ll 1$ and the fact that F_I must have the same order of magnitude as F (see Fig. 1), we observe that E_I is smaller than E by a factor r; this implies that the system can be operated with an injected field of small intensity, which is particularly convenient when the laser cavity is ring-shaped.

In Fig. 1 we compare the results obtained with Eqs. (10)–(12) in panel (a) to those obtained with Eq. (24) in panel (b). The parameters used for Eqs. (10)–(12) are listed in Table 1, and, according to the definitions of Δ, G and θ they amount to $\Delta = 2$, $G = 3$, $\theta = 4.7$, and a scaled cavity length $\eta_{\max} = 100$. For the sake of comparison we plotted the field intensities of Eqs. (10)–(12) with the same scaling adopted for Eq. (24). Therefore, in both figures the output intensity $X = |F|^2$ is plotted versus the input intensity $Y = F_I^2$ [see Eq. (22)]. The blue symbols mark the minimum and maximum intensity of the Turing patterns emerging at the modulational instability threshold, which in our system are regular rolls (see Fig. 2a in [29]), while the red symbols show the maximum intensity for the CSs. The stationary curves are indistinguishable. Two symbols are present when the CS is oscillating because the background is unstable, to indicate the minimum and maximum intensity attained by the oscillating CS. Branches of CS and Turing patterns exist according to both models, slightly more extended according to Eq. (24). We also observe that according to Eqs. (10)–(12) only oscillating CS exist.

3. Temporal localised structures and snaking ladder

In the previous sections and in our previous works, CSs existence and stability have been shown to be a robust prediction of

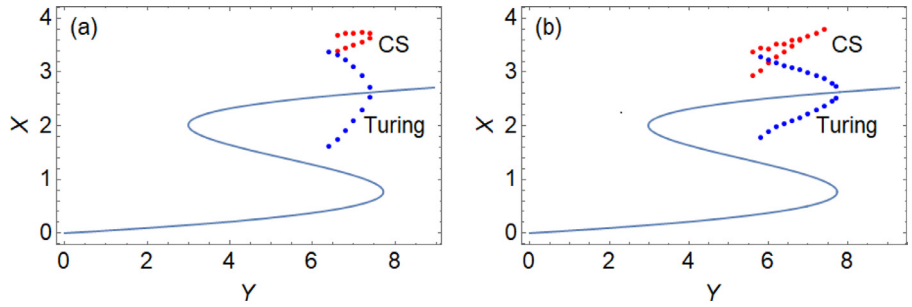

Fig. 1. Homogeneous stationary state, branch of stable CSs and Turing patterns obtained with Eqs. (10)–(12) (a) and with Eq. (24) (b). The parameters used for Eqs. (10)–(12) are listed in Table 1, the parameters for Eq. (24) are $\Delta = 2$, $G = 3$ and $\theta = 4.7$.

Table 1
Parametric set for Eqs. (10)-(12) (or, equivalently, Eqs. (6)–(8)).

θ_c	α	μ	L	τ_d	τ_p	τ_e	n	β	k''
-1.9865	2	1.005	5.8 mm	0.1 ps	100 ps	0.2 ps	3.3	0	-440 fs^2fs^2/mm

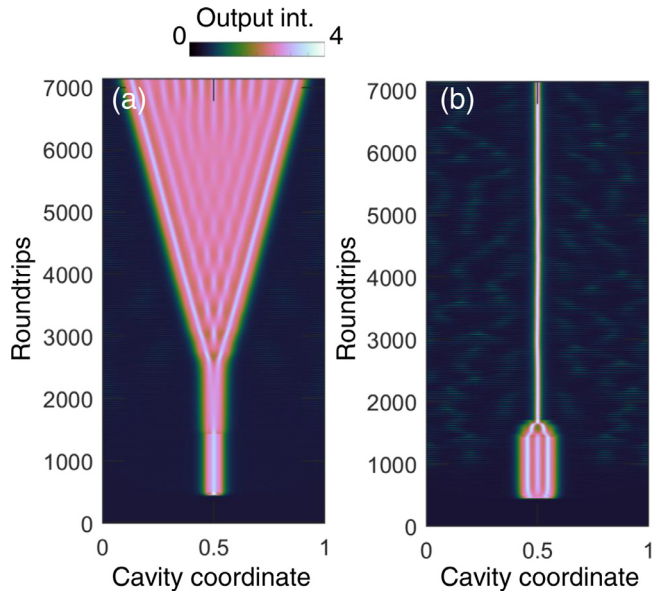

Fig. 2. A pulse with $w = 2d_{CS}$ is injected at $t = 400$ until $t = 1400$. Left: the emission switches to the roll pattern for $Y = 6.9$. Right: a broader pulse $w = 4d_{CS}$ decays to a single CS for $Y = 6.5$. The spatial coordinate is normalised to its maximum value $\eta_{\max} = 100$.

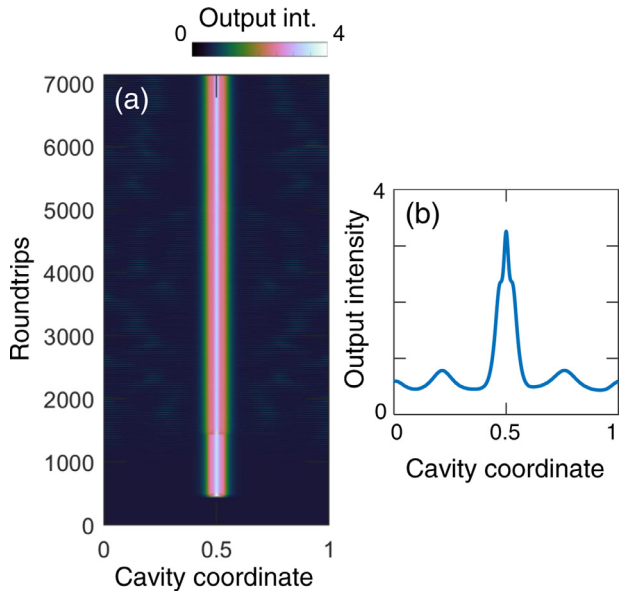

Fig. 3. $Y = 6.7$ A pulse with $w = 2d_{CS}$ is injected at $t = 400$ until $t = 1400$. (a) at regime we obtain a LS with one peak (LS_1); (b) the intensity profile reveals that the LS_1 shape and peak are different from that of the CS (see Fig.2g in [28]).

different QCL models. The proper addressing of external pulses allows to create states with a number of coexisting CSs (see Fig.8b in [29]). This property not only allows to encode information in the field profile but also allows to change the shape of the comb associated to the single CS, shown on Fig.2g in [28]. In both perspectives, it would be highly desirable to prove the existence of other classes of localised structures other than CSs, in order to widen the 'encoding alphabet'and to gain more flexibility for comb tailoring.

A cue in this direction is the well-established evidence that when a modulational instability gives rise to a global stationary patterns (rolls, in our case), there may emerge a class of LSs exhibiting a self-confined portion of the global pattern, embedded in a homogeneous background. The extent of such portion varies and since the global pattern is generally characterised by intensity peaks, the LSs differ by the number of peaks appearing in the self-confined modulated region. In our case where the global pattern is represented by 1D Turing Rolls, the LSs can be unambiguously designated by the number n of their peaks, and we will dub them LS_n in the following. Several LS_n (or even all the possible LS_n the system can sustain as stationary solution, compatibly with its spatial extension), may coexist for certain ranges of a system parameter. Since the power associated to a LS_n grows with the peak number n, a plot of the LS_n power versus the control parameter, will appear an ascending sequence of branches, one for each stable LS_n of the system (see e.g. Fig. 3 in [33]).

An analytical search for the bifurcations giving birth to the LS_n solution branches in this model is beyond the scope of our paper, but it is interesting that a thorough analysis of such solutions for the Swift-Hohenberg equation [33] or for Kerr and saturable passive optical systems [34] showed that the sequence of stable and unstable LSs are connected to the subcritically bifurcated pattern at the MI threshold and they form a winding manifold of modulated solutions (again, see Fig. 3 in [33]). When non-local effects are taken into account, the LS_n stability range is not limited within the same span of the control parameter and sweeping the latter can cause the system to realise a sequence of LS with ascending index n [35,36]. Due to the particular winding of the LS_n branches, this phenomenon has been commonly dubbed 'homoclinic snaking'.

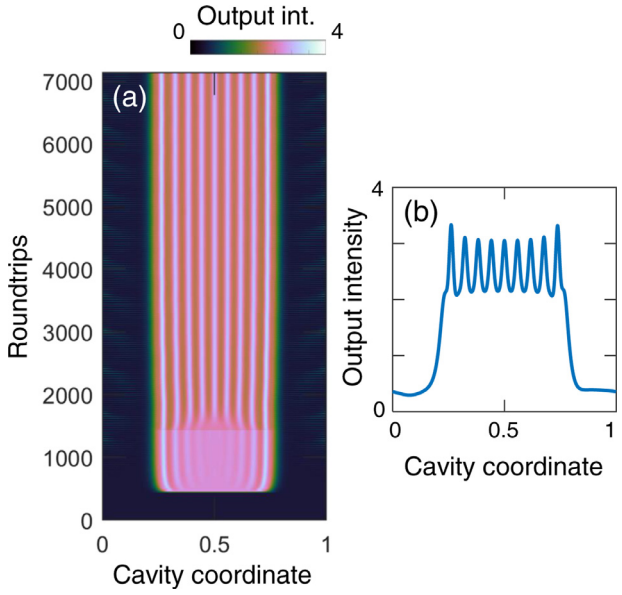

Fig. 4. $Y = 6.62$ A pulse with $w = 24d_{CS}$ is injected at $t = 400$ until $t = 1400$. (a) at regime we obtain a LS with nine peaks (LS_9); (b) the intensity profile of the LS_9.

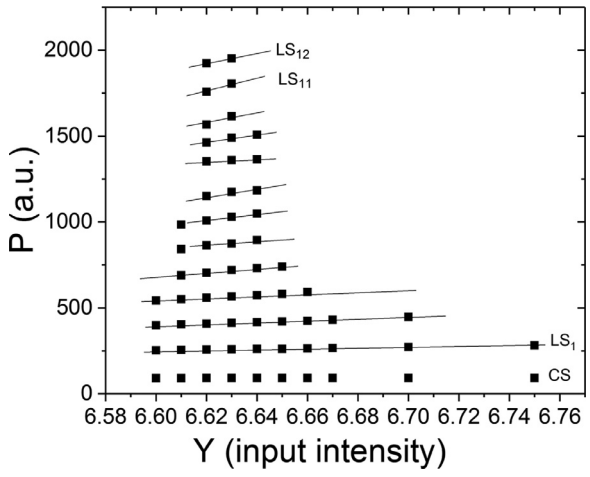

Fig. 5. The snaking ladder showing the various stable LS_n for each input intensity. The lower values correspond to the single CS, the line above them, labeled LS_1 corresponds to the structures shown in Fig. 3 and the following lines to LS of increasing index n up to 11 and 12 (labels in the upper part of the figure). The lines connecting LS of equal index at different Y are a guide for the eye.

In the case of semiconductor devices, snaking was observed experimentally in different set-ups, e.g. a semiconductor amplifier [37] and in two coupled, bidimensional, broad-area VCSELs [38].

In a fast, miniaturised laser, one can easily envisage that, by using the injected field as the control parameter, it could be possible to excite a sequence of LS_n structures which will modify the pulse sequence emitted by the laser, with obvious implications on the information encoding capability. Moreover, structures with different number of peaks will correspond to spectra with different harmonics. Spectra might then be tailored according to how many LS_n are encoded in the laser cavity and how many peaks each LS will have (and in which sequence). Also, CS can be interspersed in the field profile, together with LS_n of different indices, encoded in arbitrary sequences.

We chose the same parameter set of Section 2, since previous investigation warranted an excellent knowledge of the patter dynamics and scenery we could meet. We searched for a LS ladder by injecting pulses with the same technique used in subsection 'Switching' of [29]. We started by exciting the usual CS as described above, but we gradually increased the width of the addressing pulse w to try and excite a structure comprising two peaks at regime, after pulse extinction. In the following, as a reference unit for the pulse width w, we will consider d_{CS}, the FWHM of the CS.

We found (as hinted in subsection 'Switching' of [29]) that wherever the homogeneous solution is stable ($Y > 6.7$), a pulse significantly broader than the single CS will cause the transition to the roll pattern (Fig. 2a). This led us to search the snaking in a region where the background profile is unstable.

For $Y \leq 6.5$, no matter how broad the pulse, the formed structure after pulse extinction will invariably decay to a single CS (Fig. 2b). Successful excitation of structures corresponding to a portion of roll pattern exhibiting multiple peaks was instead achieved in the range $6.6 \leq Y \leq 6.75$, i.e. for an input field range of about 2.2%, comparable to the extensions reported on Figs. 2 and 3 in [36] and on Fig. 2 in [37], although significantly narrower than that reported on Fig. 3 in [33].

For suitable values of Y, several coexisting LS_n could be excited up to $n = 12$, by increasing the value of the pulse width w. Fig. 4 shows an example of LS_9. As it turns out, the order n of the coexisting LS_n is strongly dependent on Y, increasing from 1 for $Y < 6.55$ up to 12 at $Y = 6.62$ and decreasing again to 1 for $Y = 6.7$

Consistently with existing literature we characterised the LS_n by introducing a quantifier linked to the profile power. In this case, though, one must be careful because the background changes irregularly in space and time, so that a mere intensity integral on the cavity profile is not a reliable indicator. We introduced a power indicator P in which the profile integral included a watermark filter on the intensity, in order to remove most of the fluctuations, and was then averaged over a suitable number of independent simulations. Fig. 5 shows the ladder of LS_n versus the homogeneous input field Y. Since our system does not encompass non-local effects, it is not a surprise that the ladder is not tilted [35]. Unluckily this means that a simple sweep of the input field intensity will not be able to control an ascending or descending ramp of the number of peaks in the LSs, but it will be necessary to introduce pulses having controlled widths.

4. Conclusions

We provide a new formal approach to the modelling of an externally driven QCL showing that, in the limit of fast medium variables, an adiabatic elimination of carrier population and polarisation can be performed, retaining the descriptive capability of the complete model while remarkably reducing the computational requirements. In addition, the model we cast can be reduced to the GLLE under the same limits described in [28]. The formation of global roll structures and CS is remarkably consistent among the models. In the case of the GLLE, we show that CS are not the only stable localised structures in this laser and describe a set of multi-peaked structures corresponding to localised portions of the global rolls emerging from the modulational instability. Such evidence points to new approaches to information encoding and optical frequency comb tailoring.

Declaration of Competing Interest

The authors declare that they have no known competing financial interests or personal relationships that could have appeared to influence the work reported in this paper.

References

[1] Abraham NB, Lugiato LA, Narducci LM. Special issue on instabilities in active optical media. J Opt Soc Am B 1985;2(1).
[2] Arecchi FT, Harrison R. Instabilities and chaos in quantum optics. Berlin: Springer; 1987.
[3] Abraham NB, Arecchi FT, Lugiato LA. Instabilities and chaos in quantum optics-II. New York: Plenum; 1988.
[4] Bandy DK, Oraevsky AN, Tredicce JR. Special issue on nonlinear dynamics of lasers. J Opt Soc Am B 1988;5.
[5] Abraham NB, Firth WJ. Overview of transverse effects in nonlinear optical systems. J Opt Soc Am B 1990;7:951–62.
[6] Arecchi FT. Space-time complexity in nonlinear optics. Physica D 1991;51:450–64.
[7] Lugiato LA. Nonlinear optical structures, patterns, chaos, in chaos. Solitons and Fractals 1994;4. Ns 8/9
[8] Haken H. Synergetics - An introduction. Berlin: Springer; 1977.
[9] Nicolis G, Prigogine I. Self-organization in nonequilibrium systems. New York: Wiley; 1977.
[10] Del'Haye P, Schliesser A, Arcizet O, Wilken T, Holzwarth R, Kippenberg TJ. Optical frequency comb generation from a monolithic microresonator. Nature (London) 2007;450:1214.
[11] Herr T, Brasch V, Jost JD, Wang CY, Kondatiev NM, Gorodetsky ML, Kippenberg TJ. Temporal solitons in optical microresonators. Nat Photon 2014;8:145.
[12] Lugiato LA, Lefever R. Spatial dissipative structures in passive optical systems. Phys Rev Lett 1987;58:2209.
[13] Coen Stephane, Randle Hamish G, Sylvestre Thibaut, Erkintalo Miro. Modeling of octave-spanning Kerr frequency combs using a generalized mean-field Lugiato–Lefever model. Optics Letters 2013;38(1):37–9.
[14] Castelli F, Brambilla M, Gatti A, Prati F, Lugiato LA. The LLE, pattern formation and a novel coherent source. Eur Phys J D 2017;71:84.
[15] Lugiato LA, Prati F, Gorodetsky ML, Kippenberg TJ. From the Lugiato-Lefever equation to microresonator-based soliton Kerr frequency combs. Phylos Tran R Soc, A 2018;376:20180113.
[16] Lugiato LA, Prati F, Brambilla M. Nonlinear optical systems. Cambridge, UK: Cambridge University Press; 2015.
[17] Chembo YK. Kerr optical frequency combs: theory, applications and perspectives. Nanophotonics 2016;5:214.
[18] Kippenberg TJ, Gaeta AL, Lipson M, Gorodetsky ML. Dissipative Kerr solitons in optical microresonators. Science 2018;361:eaan8083.
[19] Piccardo M, Schwartz B, Kazakov D, Beiser M, Opacak N, Wang Y, Jha S, Hillbrand J, Tamagnone M, Cen W, Zhu A, Columbo L, Belyanin A, Capasso F. Frequency combs induced by phase turbulence. Nature (London) 2020;582:360.
[20] Meng B, Singleton M, Shahmohammadi M, Kapsalidis F, Wang R, Beck M, Faist J. Mid-infrared frequency comb from a ring quantum cascade laser. Optica 2020;7:162.
[21] Faist J, Capasso F, Sivco DL, Sirtori C, Hutchinson AL, Cho AY. Quantum cascade laser. Science 1994;264:553.
[22] Hugi A, Villares G, Blaser S, Liu HC, Faist J. Mid-infrared frequency comb based on a quantum cascade laser. Nature (London) 2012;492:229.
[23] Villares G, Hugi A, Blaser S, Faist J. Dual-comb spectroscopy based on quantum cascade laser frequency combs. Nat Commun 2014;5:5192.
[24] Coi H, Diehl L, Wu Z-K, Giovannini M, Faist J, Capasso F, Norris TB. Gain recovery dynamics and photon-driven transport in quantum cascade lasers. Phys Rev Lett 2008;100:167401.
[25] Faist J. Quantum cascade lasers. New York: Oxford University Press; 2013.
[26] Chow WW, Koch SW. Semiconductor laser fundamentals. New York: Springer; 1999.
[27] Lugiato LA, Oldano C, Narducci LM. Cooperative frequency locking and stationary spatial structures in lasers. J Opt Soc Am B 1988;5:879.
[28] Columbo L, Piccardo M, Prati F, Lugiato LA, Brambilla M, Gatti A, Silvestri C, Gioannini M, Opacak N, Schwartz B, Capasso F. Unifying frequency combs in active and passive cavities: temporal solitons in externally driven ring lasers. Phys Rev Lett 2021;126:173903.
[29] Prati F, Brambilla M, Piccardo M, Columbo LL, Silvestri C, Gioannini M, Gatti A, Lugiato LA, Capasso F. Soliton dynamics of ring quantum cascade lasers with injected signal. Nanophotonics 2021;10:195–207.
[30] Prati F, Columbo L. Long-wavelength instability in broad-area semiconductor lasers. Phys Rev A 2007;75:053811.
[31] Columbo L, Barbieri S, Sirtori C, Brambilla M. Dynamics of a broad-band quantum cascade laser: from chaos to coherent dynamics and mode-locking. Opt Express 2018;26:2829–47.
[32] Opacak N, Schwarz B. Theory of frequency-modulated combs in lasers with spatial hole burning, dispersion, and Kerr nonlinearity. Phys Rev Lett 2019;123:243902.
[33] Burke J, Knobloch E. Homoclinic snaking: structure and stability. Chaos 2007;17:037102.
[34] Gomila D, Scroggie AJ, Firth WJ. Bifurcation structure of dissipative solitons. Physica D 2007;227:70–7.
[35] Firth WJ, Columbo L, Maggipinto T. On homoclinic snaking in optical systems. Chaos 2007;17:037115.
[36] Firth WJ, Columbo L, Scroggie AJ. Proposed resolution of theory-experiment discrepancy in homoclinic snaking. Phys Rev Lett 2007;99:104503.
[37] Barbay S, Hachair X, Elsass T, Sagnes I, Kuszelewicz R. Homoclinic snaking in a semiconductor-based optical system. Phys Rev Lett 2008;101:253902.
[38] Genevet P, Turconi M, Barland S, Giudici M, Tredicce J. Bifurcation diagram and control of localized laser structures. J Nonlinear Opt Phys 2012;21:1250029.